https://doi.org/10.5194/egusphere-2026-2108
Preprint. Discussion started: 12 August 2026

Rain gauge aerodynamic design to minimise wind-induced bias in precipitation measurement

Enrico Chinchella[1], Arianna Cauteruccio[1,2], Pak-Wai Chan[3], Luca G. Lanza[1,2]

[1] Department of Civil, Chemical and Environmental Engineering, University of Genova, Genoa, Italy
[2] WMO Measurement Lead Centre "B. Castelli" on Precipitation Intensity, Genoa, Italy
[3] Hong Kong Observatory, Hong Kong, Hong Kong SAR, China

Correspondence to: Enrico Chinchella (enrico.chinchella@edu.unige.it)

Abstract. The presence of wind introduces biases in precipitation measurements obtained from traditional rain gauges due to the interaction between the airflow and the outer shell of the instrument, which acts like a bluff body immersed in a wind stream. The airflow is diverted, creating an updraft and accelerating the flow velocity. This interacts with the fall trajectories of hydrometeors near the gauge rim, causing some to deviate out of the collector. The resulting wind-induced undercatch can be minimised by adopting a suitable design for the outer shell of the gauge. While the effectiveness of an inverted conical shape for the outer walls of the gauge has already been demonstrated in the literature, this work proves that the size and geometric profile of the collector's rim are crucial in reducing the effect of wind on precipitation measurements. Building on the construction requirements derived from operational constraints, various single and dual inclination rim profiles were tested using computational fluid dynamics simulation and Lagrangian particle tracking to identify the most effective design. The proposed rim profile is then thoroughly tested in numerical simulations performed over an extended range of wind speeds and precipitation intensities. The scalability of the rim profile to suit different sizes of the collector area is demonstrated, and adjustment curves are obtained to address residual bias. A comparison with existing high-performance gauges on the market revealed that the proposed design significantly outperforms existing solutions.

1 Introduction

The wind-induced bias of precipitation measurements using catching rain gauges (Cauteruccio et al., 2021) is due to the interaction between the airflow pattern developing around and above the gauge collector and falling hydrometeors of various size and numerosity. Control variables are linked to the physical characteristics of both the precipitation process, especially the particle and velocity distribution, and the instrument design, basically the size and shape of the outer envelope.

The airflow velocity pattern is induced by the bluff-body behaviour of the instrument when immersed in the wind field, and the detailed streamflow is determined by the outer geometry of the gauge body. The lateral profile of the gauge walls and the design of the collector's edge (the upper rim) are critical geometric features for generating updraft, acceleration and turbulence near the collector. Meanwhile, the typical radial symmetry of catching rain gauges allows the influence of wind direction to be neglected.

https://doi.org/10.5194/egusphere-2026-2108
Preprint. Discussion started: 12 August 2026

In the past, indications on how to improve the gauge performance in windy conditions by adapting the gauge design were obtained from experimental campaigns (see Folland, 1988; Strangeways, 2004) or wind tunnel tests (see e.g. Robinson and Rodda, 1969; Green and Helliwell, 1972), and some manufacturers already introduced the so-called "aerodynamic" gauge shape in their commercial products (see EML, 2017; Davis Instruments, 2022). Meanwhile, the literature also proposed some custom geometries to suit specific applications (see e.g., Hasse et al., 1998). The main outcome of such experiments was to demonstrate that the cylindrical shape used for most commercial rain gauges creates too abrupt an obstruction to the airflow, with strong updraft and acceleration above the gauge collector, resulting in a significant undercatch of the precipitation amount.

An inverted conical shape was identified (Strangeways, 2004) as a technically feasible solution to minimise the aerodynamic disturbance induced by the instrument on the surrounding airflow, and such an indication was realized in practice by designing "hourglass" shapes, which allow maintaining inverted conical profile in the top part of the gauge (close to the collector), while enclosing the instrument mechanics (typically the tipping-bucket mechanism) into the lower part of the gauge.

In the literature, both hardware and software solutions have been developed to minimise and correct wind-induced bias. Wind shields were tested in the field and in the wind tunnel, and the associated benefit of reduced undercatch was quantified by comparing precipitation measurements obtained from shielded and unshielded gauges (Lindroth, 1991; Seibert and Morén, 1999; Kochendorfer et al., 2017).

Being rather bulky, windshields require sufficient space around the gauge collector for installation, which is not always available in operational conditions. They also require sufficient distance from other objects, trees and vertical surfaces on site. For reasons of space and cost, windshields are often used at experimental sites. Using them across a large rain gauge network incurs a significant additional financial cost. Furthermore, while windshields are effective in reducing wind-induced bias, they cannot eliminate it entirely. While they minimise the flow acceleration and updraft above the gauge collector, turbulence develops more strongly than with an unshielded gauge. This significantly affects the trajectories of lighter hydrometeors.

The use of computational fluid dynamics (CFD) and parallel computing, largely used in industry for aerodynamic design, was introduced in the study of rain gauges as well, with reference to the aerodynamic performance of the gauge when immersed in a wind flow (Nešpor and Sevruk, 1999).

Recently, Colli et al. (2018) presented a CFD-based comparison of the aerodynamic performance of various commercial rain gauges, showing not only that the inverted conical (so-called "aerodynamic") shape outperforms all other commonly used designs, but also that the "chimney" shape used for weighing gauges is even less performant than the cylindrical shape. That study also highlighted the relevance of the collector's rim design on the aerodynamic performance of the gauge.

The implementation of numerically derived adjustment curves in real time or a posteriori (see, for example, Habib et al., 1999) allows precipitation measurements affected by wind-induced bias to be adjusted. However, both hardware and software solutions are subject to some unavoidable drawbacks.

https://doi.org/10.5194/egusphere-2026-2108
Preprint. Discussion started: 12 August 2026

Using adjustment curves requires a co-located anemometer and measurements of both precipitation and wind at very high temporal resolution, preferably at one-minute intervals. The less accurate the temporal resolution, the less accurate the correction applied. In this case, the raw measurements are subject to inherent wind-induced bias. Correction and interpretation depend heavily on the user's awareness and technical capabilities.

The use of hardware and software solutions can result in significant variations in the homogeneity of precipitation time series. The temporary installation of windshields or applying correction procedures to recent data only, or in the absence of simultaneous high-resolution wind measurements, introduces a factor of non-homogeneity into the time series.

Coupling CFD analysis with numerical optimization does improve designs more effectively (Martins, 2022) by enlarging the testing possibilities and exploiting parameterization of the gauge geometry to identify the most efficient design details. The approach has been widely used for decades in fluid mechanics (Pironneau, 1974), aerospace science and technology (He et al., 2019), wind turbines optimization (Dhert et al., 2017), but was not yet adopted in rain gauge design.

The development and use of an aerodynamically shaped rain gauge that can minimise the effects of wind, in terms of both flow acceleration and updraft, could be the optimal solution. It is a compact, hardware solution that requires no more costly installation or manufacturing procedures than a traditional cylindrical rain gauge. It is also suitable for remote installations where no co-located wind measurements are available and where data is recorded at a coarse time resolution. If a very high level of accuracy is required, however, the need to record precipitation and wind at a high resolution (at least one minute) persists.

In this paper, we use CFD-based aerodynamic design to improve the performance of catching gauges in taking accurate rainfall measurements when wind is also present. The work aims to demonstrate that aerodynamic design based on numerical simulation can further improve the performance of catching rain gauges, beyond the already existing performant solutions.

The paper is organised as follows: Section 2 presents the design methodology, starting with an overview of the operational constraints. It describes the parameterisation assumed for the gauge geometry and defines the performance indicator adopted to assess the instrument's performance in minimising wind-induced bias. Section 3 describes the numerical simulation results and provides an evaluation of the various proposed design solutions. It also provides a comparison with existing commercially available gauge designs that have demonstrated good performance. In Section 4, the most efficient solution identified using performance indicators is characterised in detail for a wide range of wind speed and precipitation intensity conditions, addressing both rainfall and snowfall measurements. Its scalability to gauges with a different collector area is proven, and suitable adjustment curves are derived that allow the residual bias to be treated a posteriori. The conclusions of the present work are then drawn in Section 5.

2 Methodology

This study proposes and compares various radially symmetric profiles of the collector of a catching-type precipitation gauge, with the aim of defining a design solution that minimises the amount of precipitation lost in windy conditions, known as

https://doi.org/10.5194/egusphere-2026-2108
Preprint. Discussion started: 12 August 2026

wind-induced undercatch. We make no specific hypotheses about the measuring principle of the gauge, since this does not affect the amount of precipitation collected, but only its ability to quantify this amount or intensity. Practical constraints are considered to manufacture the gauge easily and to limit further sources of error that are not explicitly quantified in this work, such as splashing and snow capping. Different versions of the gauge collector edge are proposed, with an increased level of complexity in the profile and a greater number of parameters considered in the design procedure. The performance of the proposed versions in limiting wind-induced undercatch is compared with that of the most efficient commercially available gauges.

2.1 Geometric constraints and new design of the collector's edge

The most important geometric specification for a catching gauge (CG) is the size of the collector's area. In general, small size gauges would cause less obstruction to the wind flow. However, the aerodynamic 'bluff-body' behaviour of the gauge is expected to be quite scalable within a reasonable range, and the wind-induced bias is mostly determined by the outer profile of the gauge body as a whole (see e.g., Cauteruccio et al., 2024). As stated in the World Meteorological Organization's (WMO) Guide to Instruments and Methods of Observation (WMO, 2024), while the recommended collector area for manual or weighting gauges is 200 cm², larger collector sizes are preferable, especially when measuring solid precipitation. The justification for this is given in the same guide, which states that 'gauges with a large collector orifice (or opening) should have lower statistical error in their measurements'. Similar considerations hold for tipping-bucket and floating gauges. Furthermore, a larger collector area may also reduce the error due to splashing and the probability of snow capping. This is because these effects, which are mostly caused by precipitation interacting with the collector's rim, become less significant as the collector's area increases.

Nitu and Wong (2010) conducted a survey of gauge specifications in use by National Weather and Hydrological Services (NWHS) among WMO member countries, reporting a slight prevalence of gauges with a collector area between 300 and 500 cm². We consulted the catalogues of 27 rain gauge manufacturers to determine the most popular collector area. The results are as follows: for an area of less than 300 cm2, 20 models were found, the most common of which by far is 200 cm2. A total of 30 models were found with a collector area between 300 and 500 cm², with 400 cm² being the most common. Finally, 11 models were found for an area larger than 500 cm², the most common of which is 1000 cm². Based on these results, we assumed a collector area of 400 cm² for this study, although tests were conducted to evaluate the scalability of the proposed geometry towards a 200 cm² gauge, the second most common size.

The WMO recommendations provide a relevant geometrical constraint about the gauge geometry. According to the WMO Guide (WMO, 2024), the internal wall of the collector should be sufficiently steep to prevent splashing, both internally and externally. This can be achieved by shaping the internal collector so that, at every point, any line normal to its inner surface lies inside and below the rim. To meet these recommendations, the inner wall of the gauge collector was designed to be ogival in shape. Starting at the top, the profile was obtained by drawing a 30° arc centred on the opposite side of the rim,

https://doi.org/10.5194/egusphere-2026-2108
Preprint. Discussion started: 12 August 2026

which was then connected tangentially to a straight line inclined at 60° to the horizontal until the bottom orifice was reached (see Fig. 1a). The internal surface is then obtained by revolving this line through 360° around the vertical axis.

The ogival shape is also effective in reducing the aerodynamic disturbance above the collector since it behaves like an inverted conical shape, which had already been proven to be quite effective (Cauteruccio et al., 2024). The outer shell of the proposed gauge was therefore designed to follow the internal ogival shape, with an intermediate empty space of few millimetres between them to allow for the installation of a heating element, should it be required (see Fig. 1a).

Given the geometrical constraints of the overall design, further optimization of the aerodynamic performance is obtained here by focusing on the design of the collector's rim. This is indeed a key feature of the profile, able to significantly influence the airflow pattern above the gauge collector, including acceleration and updraft, which determine the wind-induced undercatch. A suitable parameterization of the rim profile is defined to this aim, and an incremental stepwise approach is used to evaluate the influence of different rim profile parameters on the gauge performance in windy conditions.

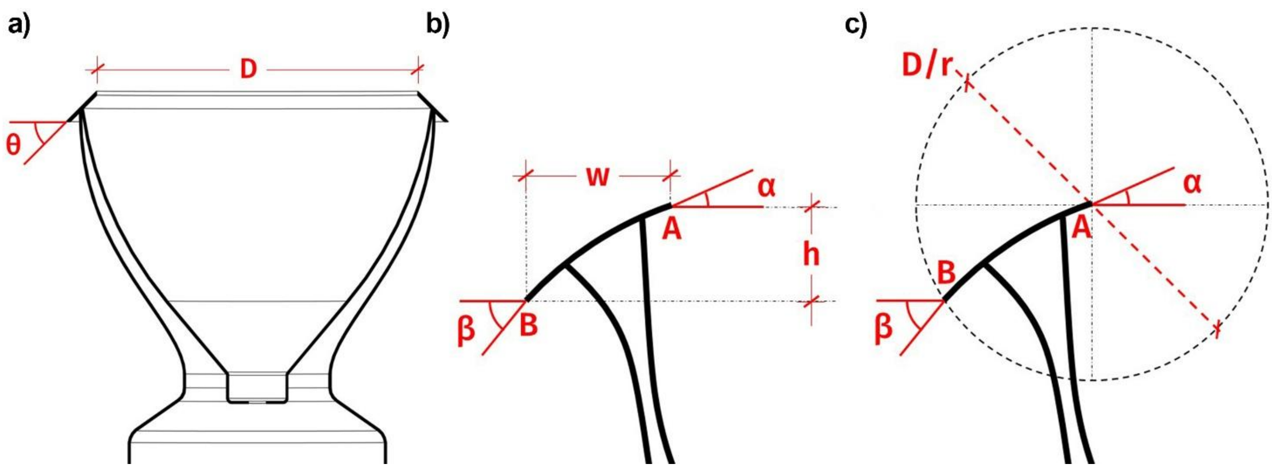

Figure 1: a) Cross-section of the proposed gauge design, having a collector's diameter D, showing the inner ogival profile and the outer shell. The initial straight rim is inclined by an angle q to the horizontal. b) Proposed rim profile featuring fixed thickness, h, variable width, w, and double inclination with an inflow angle b and an outflow angle a. c) Proposed rim design featuring double inclination and variable thickness, as a function of the fractional arc span, r.

First, the response of a straight rim profile at different inclination angles (θ = 30°, 45° and 60°) relative to the horizontal has been tested. Figure 1a shows an example for θ = 45°. This simple design is currently used in some commercially available rain gauges because it can easily be made from any construction material and improves performance in windy conditions compared to the vertical edge (θ = 90°) found in some low-performance weighing gauges. However, in commercial gauges, the inclined rim starts typically flush with the outer vertical wall of the cylindrical shell, rather than projecting beyond it. In this configuration, the inflow angle (the angle of an inclined solid profile relative to the horizontal at the upstream edge) and the outflow angle (the angle of an inclined solid profile relative to the horizontal at the downstream edge) are identical.

https://doi.org/10.5194/egusphere-2026-2108
Preprint. Discussion started: 12 August 2026

In a second step, we tested the aerodynamic behaviour of a rim profile with a fixed thickness and double inclination, i.e. with an inflow angle β that differs from the outflow angle α, while keeping the rim thickness (h) equal to a fixed value. Figure 1b shows a sketch of this configuration. The design assumes that the rim is shaped as an arc of a circle starting at the internal edge of the collector (A), where it is tangent to a segment inclined at an angle equal to the outflow angle (α). This arc then extends outwards until it reaches a plane located 20 mm below the collector's rim (B), which is tangent to a segment inclined at an angle equal to the inflow angle (β). Varying α and β changes the width of the rim (w), while the vertical obstruction h (normal to the horizontal wind) at the stagnation point remains constant. Three values of the outflow angle (α), equal to 10°, 20° and 30°, were tested, as were two values of the inflow angle (β), equal to 45° and 60°.

Finally, we tested a rim design featuring double inclination and variable thickness. In this design, both the length of the arc (related to the thickness, h) and the outflow angle (α) are adjustable. Figure 1c shows a sketch of this configuration. The inflow angle was fixed to β = 45°. The fractional arc span (r) is defined as the ratio of the gauge collector's diameter to the diameter of a circle centred at A, which defines the rim's outward extension and the position of point B (see Fig. 1c). This approach made scaling the proposed geometry to different collector sizes easier. The vertical obstruction (normal to the wind direction) at the stagnation point varies between simulations. Four values of α were tested, equal to 0°, 10°, 20° and 30° meanwhile for the normalised arc length five values were considered equal to r = 1.5, 2, 2.5, 3 and 4.

2.2 Performance indicator

The Catch Ratio (CR), obtained by means of CFD simulation, is the performance indicator selected for comparing the proposed design variants. The CR is defined as the ratio of the number of particles (hydrometeors) of a given diameter collected by the gauge in windy conditions to the number of particles of the same diameter that would have been collected in the absence of wind disturbance. A CR value of 1 indicates the absence of wind-induced bias, while lower values suggest undercatch and higher values suggest overcatch. A CR value of 0 means that the gauge does not collect any particle of the given diameter.

To quantify the wind-induced bias of CGs a two-step numerical approach is employed. Initially a CFD simulation model is used to evaluate the airflow features around the gauge body. CFD simulations were run using the OpenFOAM C++ library (Jasak, 2009) to numerically solve the Unsteady Reynolds Averaged Navier-Stokes (URANS) equations. Simulations were run considering a wind speed (U_{ref}) of 5 m s^{-1}, that is a common occurrence in the field. In the simulations air was considered as an incompressible fluid with a density ρ of 1.2 kg m^{-3} and a kinematic viscosity ν of $5x10^{-5}$ m^2 s^{-1}. A local-timestepping approach (Jeanmasson et al., 2019) was used to force the simulation toward a steady state condition while reducing the computational cost. Turbulence was solved using the k-ω SST model (Menter, 1994).

The simulation domain is maintained constant throughout all simulations and is 3 m wide, 5 m long and has a height of 2.5 m. The centre of the gauge collector is positioned in the origin of the axes, that are oriented with the X axis parallel to the wind direction and the Z axis directed upward. Standard boundary conditions for external aerodynamic problems were set with a fixed inlet velocity and a fixed outlet pressure. For the remaining boundary limits a slip condition is set while a no-

https://doi.org/10.5194/egusphere-2026-2108
Preprint. Discussion started: 12 August 2026

slip condition is imposed on the gauge surface. For k and ω, y^+-independent wall functions are used (Liu, 2016). Finally, the domain is discretized using hexahedral cells 10 cm in size, that were progressively refined close to the gauge body and in its wake up to about 1 mm. This resulted in meshes having about 5.2 million cells.

A Lagrangian Particle Tracking (LPT) model was used to simulate the trajectories of particles approaching the gauge collector. This model solves the equation of motion for each hydrometeor released within the computational domain and subject to the effects of gravity and aerodynamic forces. In particular, the drag force was modelled using the same formulation as that used by Cauteruccio et al. (2024). An uncoupled approach is used for the simulations, meaning that trajectories were computed considering the steady state velocity field neglecting particle to particle interaction. For each geometry six liquid particle diameters were simulated, equal to 0.25, 0.5, 0.75, 1, 2 and 3 mm, those most affected by wind. The releasing positions were set in the domain in regularly spaced grids, so that the particle positioned on the centre of the grid would reach the centre of the collector in the absence of any aerodynamic disturbance. The grid length was increased for small diameter particles and high wind speeds to ensure that all possible trajectories are accounted for in the simulation.

For the selected gauge design providing optimal performance, liquid and solid precipitation are modelled by considering equivolumetric particle diameters equal to 0.25, 0.5, 0.75 mm and from 1 to 8 mm at 1 mm increments and for wind speeds between 1 and 20 m s^{-1}. We assume spherical particles with unit density for drops, while density is expressed by a power law formulation as a function of the particle diameter for solid particles, with a coefficient equal to 0.017 (gr cm^{-3}) and an exponent equal to -1 (Rasmussen et al., 1999). The density characteristics of dry snow are used, due to its high sensitivity to aerodynamic effects.

Hydrometeors are inserted into the simulated airflow field with an initial horizontal velocity component equal to the undisturbed wind velocity and a vertical velocity component equal to the particle terminal velocity. The terminal velocity is obtained once the gravitational force and the aerodynamic force (due to drag) are in equilibrium, meaning that the particle cannot accelerate further. To maintain consistency with the numerical model, the terminal velocity was computed by using the drag coefficient derived from the work of Cauteruccio et al. (2024).

3 Results and discussion

The airflow features and the CRs derived for each proposed design solution were compared with those of three commonly available gauges with different outer shapes as reported in the work of Cauteruccio et al. (2024). The Lambrecht rain[e]H3 cylindrical gauge, the EML SBS-500 inverted-conical gauge and the AES Nipher shielded gauge were considered. The cylindrical gauge is representative of the most typical type of gauge that is installed in the field. The inverted-conical gauge has an aerodynamic profile, with a shape that was partially optimized in previous studies for windy conditions (Strangeways, 2004). Finally, the gauge equipped with a large-diameter Nipher wind shield was optimized in the past (Nipher, 1878) to minimise the wind-induced bias when solid precipitation, which is much more affected by wind than rainfall, is expected.

https://doi.org/10.5194/egusphere-2026-2108
Preprint. Discussion started: 12 August 2026

The results are presented below, considering both the aerodynamic disturbance above the gauge collector and the resulting CR. The former is visualised through airflow velocity maps and in terms of the position and magnitude of the separation layer formed over the gauge collector. This region of accelerated flow is primarily responsible for diverting particle trajectories. Its position can be visualised as the set of points above the collector with the maximum velocity. The greater the distance between the collector and the separation layer, and the wider and faster the layer is, the greater the deflection effect on the particle's trajectories.

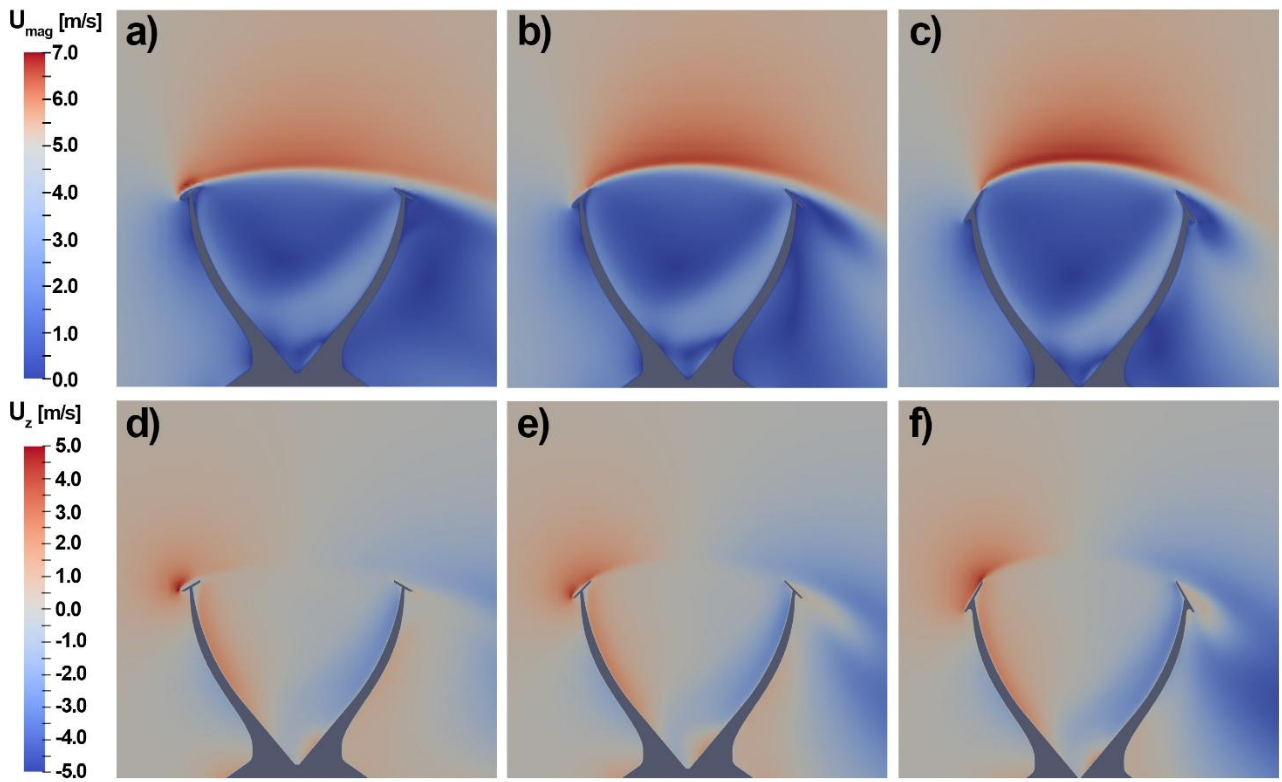

Figure 2: Airflow field in the central cross section parallel to the wind direction (X axis, wind blows from left to right) showing the velocity magnitude (U_{mag}), top panels, and the vertical velocity component (U_z), bottom panels, for a straight rim profile with ϑ equal to 30° (a, d), 45° (b, e) and 60° (c, f).

3.1 Straight rim profile at different constant inclinations

Figure 2 shows the velocity airflow fields for the three initial designs tested, considering both the velocity magnitude (panels a, b and c) and the vertical velocity component (panels d, e and f) in a central cross-section taken along the wind direction. Notable differences in the position of the boundary layer above the gauge collector are evident. For ϑ = 30°, the boundary

https://doi.org/10.5194/egusphere-2026-2108
Preprint. Discussion started: 12 August 2026

layer detaches from the rim inflow edge; for ϑ = 45°, it remains mostly attached; and for ϑ = 60°, it is fully attached. As ϑ increases, the accelerated zone and the updraft become more intense.

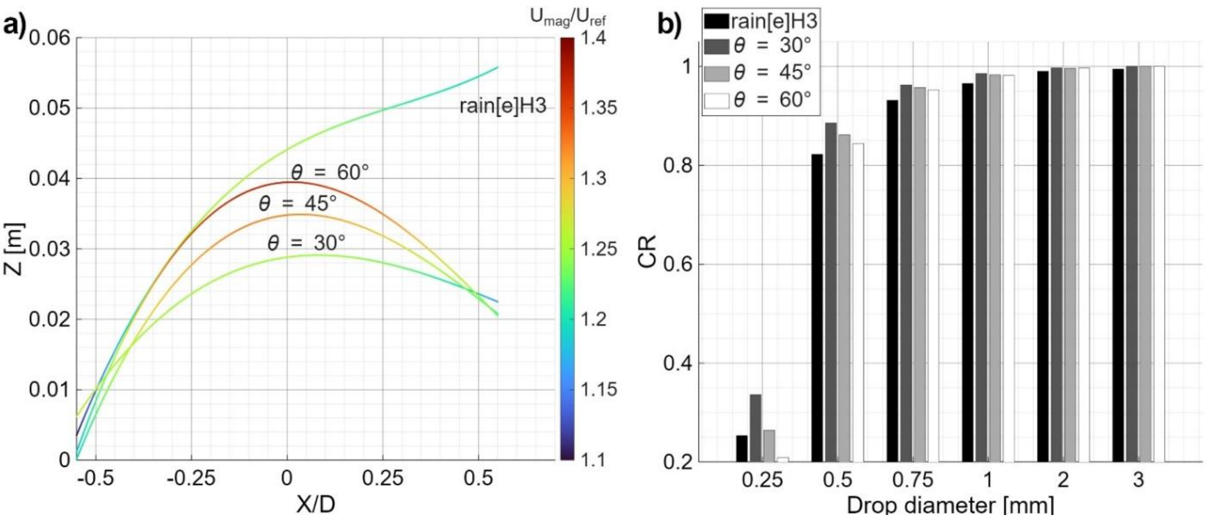

Figure 3: a) Position and normalised magnitude of the maximum flow acceleration over the gauge collector for different simulated rim designs. b) Comparison of the CRs obtained for increasing particle diameters and different simulated designs. In both cases, the performance is compared with that of the Lambrecht rain[e]H3 cylindrical gauge.

Figures 3a and 3b show the quantitative results for airflow acceleration and CR, respectively, and compare them with those of the Lambrecht rain[e] cylindrical gauge. In terms of the position of the separation layer, the Lambrecht rain[e]H3 and the proposed gauge design with a straight rim inclined at 60° are very similar up to approximately one quarter of the gauge diameter (x/D = –0.25). This behaviour is expected since the Lambrecht rain[e]H3 has a prominent rim with an inclination very close to 60°. Meanwhile in terms of the strength of the aerodynamic disturbance, the configuration at ϑ = 60° exhibits higher flow velocity values. The three proposed designs, far from the rim, present a significantly lower separation layer position, which is lower the shallower the inclination angle. Similarly, the maximum flow velocity decreases as ϑ decreases. The effect of the airflow features on the tested designs shows that the CRs approach unity as the inclination angle decreases. Comparing the CRs with those of the Lambrecht rain[e]H3 shows that the proposed gauge designs outperform the commercial gauge for all drop diameters except the smallest when ϑ = 60°.

3.2 Rim profile with double inclination and fixed thickness

Initial tests on the three preliminary rim designs discussed in the previous paragraph demonstrated the relevant role of rim inclination, with shallower angles producing better results. However, when ϑ is set to 30°, the boundary layer tends to detach from the rim's surface, which reduces the ability to control its position through the shape of the rim alone when wind speed varies. For this reason, a curved design was tested to enable a relatively shallow angle while keeping the boundary layer

https://doi.org/10.5194/egusphere-2026-2108
Preprint. Discussion started: 12 August 2026

close to the rim surface. The results for the six tested rim designs are presented in Fig. 4 and 5, showing the aerodynamic disturbance and the CRs, respectively.

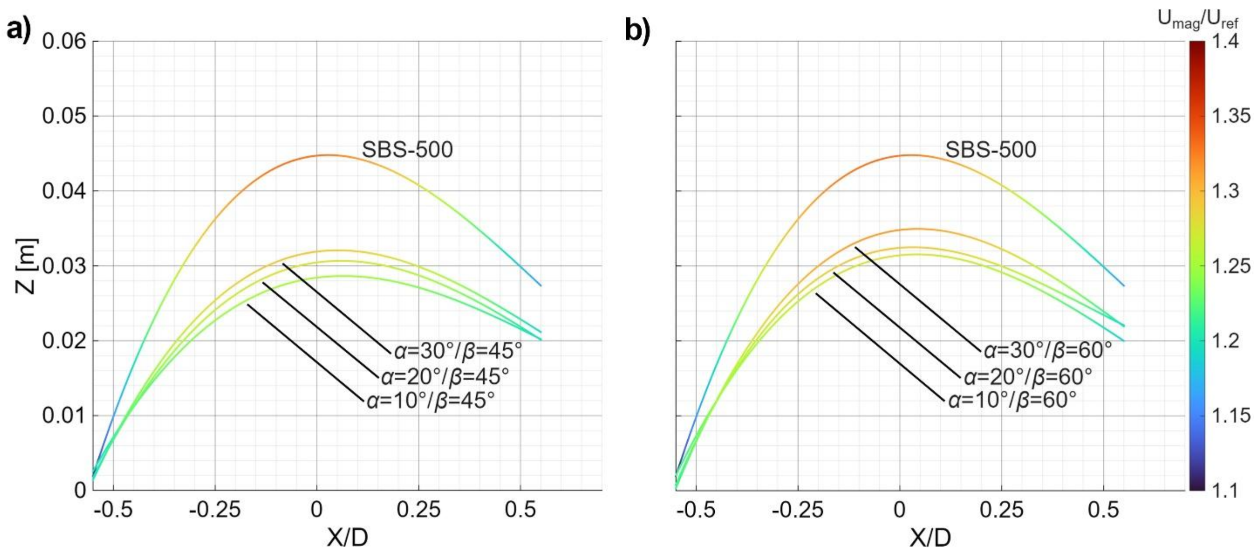

Figure 4: Position and normalized magnitude of the maximum flow acceleration above the gauge collector for different outflow angles α and β = 45° (a) or β = 60° (b). In both cases, the performance is compared with that of the aerodynamic EML SBS-500 gauge.

The results for an inflow angle of β = 60° (Fig. 4a) show the separation layer to be in a slightly higher position than the results for an inflow angle of β = 45° (Fig. 4b). However, both are significantly lower than the EML SBS-500's separation layer. In terms of flow acceleration, the proposed rim designs perform similarly to or better than the EML SBS-500, which has an inclined but very thin rim. While the effect of varying the outflow angle is less pronounced than that of the inflow angle, it is still significant.

https://doi.org/10.5194/egusphere-2026-2108
Preprint. Discussion started: 12 August 2026

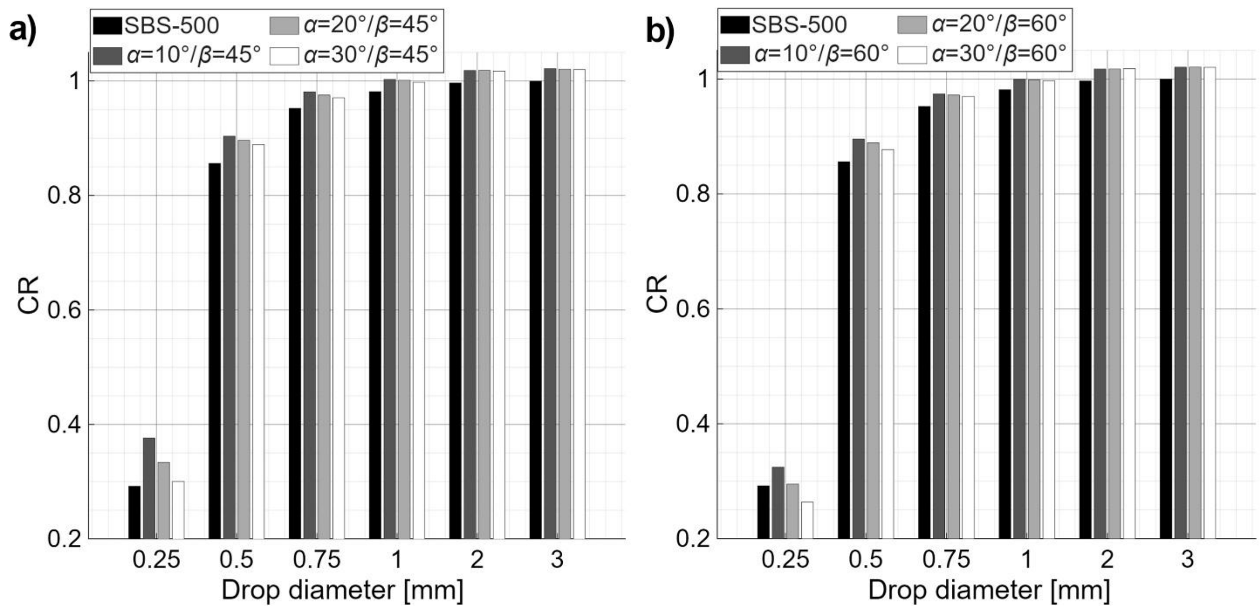

Figure 5: Comparison of CR values as a function of drop diameter for the proposed rim designs, considering different outflow angles α and β = 45° (a) or β = 60° (b). The performance indicator is compared in both cases with that of the aerodynamic EML SBS-500 gauge.

When considering the CRs (see Fig. 5), the proposed rim designs behave very similarly for drop diameters above 0.5 mm, while differences are evident for the smallest drops. The results are similar to those previously observed in terms of aerodynamic disturbance, with CRs increasing for shallower inflow and outflow angles. When compared with CRs from the EML SBS-500, slightly higher values are obtained for all drop diameters (except for $\beta = 60°$ and $\alpha = 30°$ for the smallest drop diameter). However, this also results in limited overestimation for larger drops, which is not present for the commercial gauge. A limitation of the most effective solutions is the considerable width of the collector rim. For the configuration with $\beta = 45°$ and $\alpha = 10°$, this reaches 44 mm.

3.3 Rim profile with double inclination and variable thickness

Previous results demonstrated that, despite the disadvantage of its large width, a shallow rim inclination performs better in windy conditions. The effect of different rim widths on the final geometry was therefore evaluated by fixing the normalised arc span (r) while maintaining a constant inflow angle ($\beta = 45°$). Figure 6 shows the aerodynamic disturbance for the proposed rim design solutions.

https://doi.org/10.5194/egusphere-2026-2108
Preprint. Discussion started: 12 August 2026

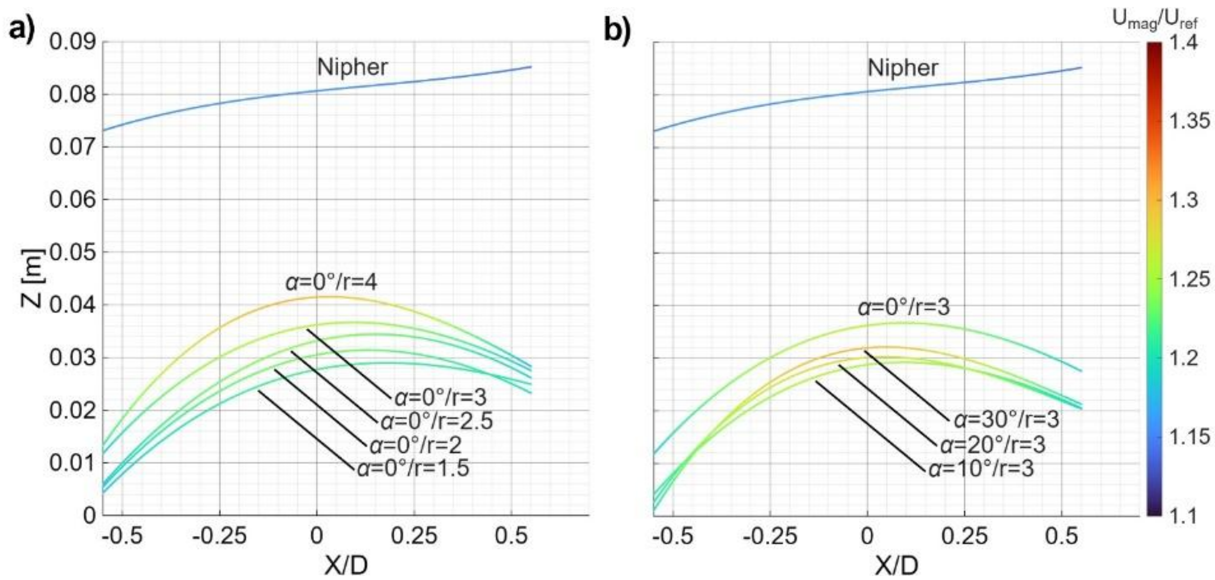

Figure 6: a) Position and normalised magnitude (with U_{ref} the undisturbed wind speed) of the maximum flow acceleration over the gauge collector for α = 0° and different normalised arc spans (r). b) Position and normalised magnitude of the maximum flow acceleration over the gauge collector for a fixed normalised arc length (r = 3) and different outflow angle α. In both cases, the performance is compared with that of a cylindrical gauge collector installed within the AES Nipher shield.

Figure 6a illustrates how changing the width of the rim (expressed in terms of the normalised arc span, r) affects the position of the separation layer. Larger rims tend to produce lower separation layers and limited flow acceleration. A jump in the upstream position of the separation layer is visible between the configuration with r = 2.5 and r = 3 and is due to the detachment of the boundary layer. This behaviour is evident in rim designs with a narrow width and shallow outflow angle but absent in other cases. Figure 6b, on the other hand, shows that when no detachment occurs, the position of the separation layer remains almost constant, while significant changes are visible in the flow acceleration, which increases with narrower rims and steeper angles. In both figures, the separation layer of the gauge collector installed within the AES Nipher shield is consistently higher, despite the significantly lower flow acceleration. This is due to the large windshield installed around the collector, which significantly modifies the flow.

https://doi.org/10.5194/egusphere-2026-2108
Preprint. Discussion started: 12 August 2026

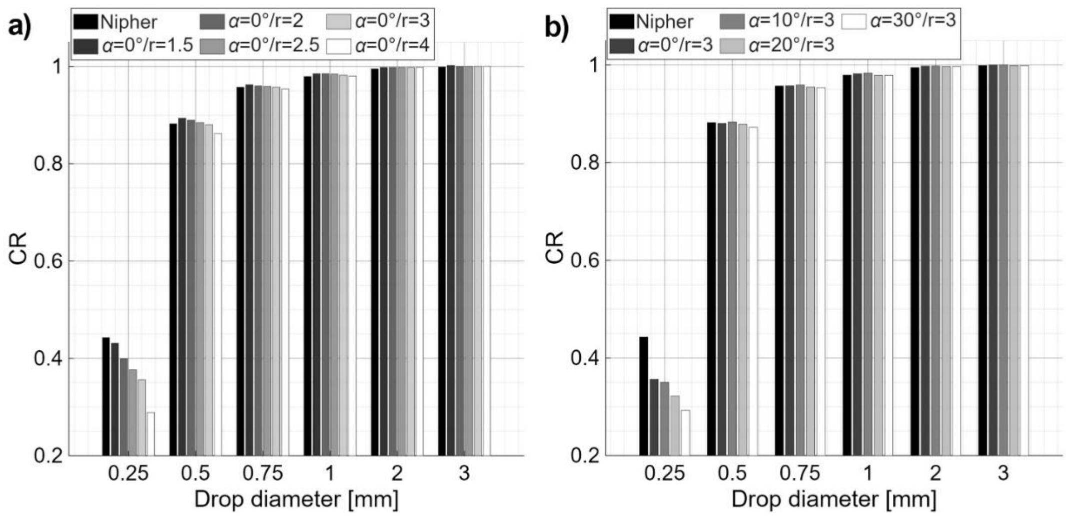

Figure 7: a) Comparison of CR values as a function of drop diameter for the proposed rim designs considering α = 0° and different normalised arc length (r). b) Comparison of CR values as a function of drop diameter for the proposed rim design considering a fixed rim width (r = 3) and different outflow angles (α). In both cases, the performance indicator is compared with that of the cylindrical gauge collector installed within the AES Nipher shield.

The impact of the observed airflow features is reflected in the values of the calculated CR shown in Fig. 7. The proposed rim designs, which do not involve separation layer detachment, exhibit very similar CR values for all drop diameters, except for the smallest diameter, when compared with the values for the cylindrical collector installed within the AES Nipher shield. From Fig. 7a, the best-performing geometry can be identified as having an outflow angle of α = 0° and a normalised arc span of r = 1.5. This design slightly outperforms the AES Nipher shielded gauge for drop diameters of 0.5 mm or above and does not exhibit overcatch for larger diameters, as observed previously. However, this design solution also results in a very large rim width.

4 Performance of the final and scaled designs

Based on the numerical results presented in the previous section, a large rim with an outflow angle of 0° minimises the overall flow disturbance above the gauge collector and, consequently, the resulting wind-induced bias. However, implementing this optimal solution would result in a rim width that is incompatible with the environmental conditions experienced by the gauge in the field. In fact, a flat rim would significantly increase splashing and the formation of snow capping, as well as the conveyance of debris from the rim surface into the collector. Furthermore, low values of r could result in a relatively fragile construction that would compromise the durability of the collector in field installations.

To reconcile the significant reduction obtained in wind-induced bias with practical requirements, the proposed optimal configuration is a rim profile with inflow and outflow angles of 45° and 10°, respectively, and a normalized arc span of 3, corresponding to a rim width of about 33 mm for the gauge with a collector's diameter of 400 mm. Numerical simulations

https://doi.org/10.5194/egusphere-2026-2108
Preprint. Discussion started: 12 August 2026

were run using the selected solution over an extended range of wind speeds (1–20 m/s) and both liquid and solid particle diameters (0.25–8 mm), as typically encountered in the field. The results are presented below.

A scaled geometry with a collector area of 200 cm² was designed using the selected parameters, and dedicated simulations were run to quantify its performance. Figure 8a illustrates the velocity field across a central cross-section of the scaled geometry, aligned with the direction of the undisturbed wind. Figure 8b compares the position and intensity of the maximum flow acceleration above the collector for the two scaled versions of the optimal geometry. The performance of the commercially available EML SBS-500 aerodynamic gauge is also reported for reference purposes.

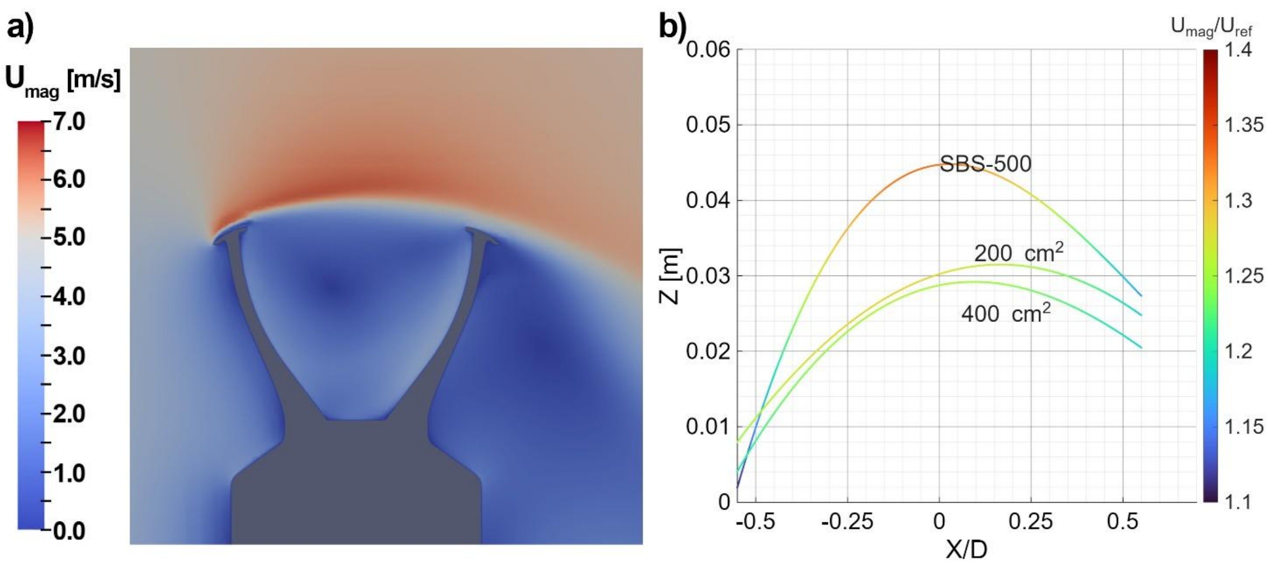

Figure 8: (a) Airflow velocity field in the central cross section parallel to the wind direction (X axis; wind blows from left to right), showing the velocity magnitude (U_{mag}) for the scaled gauge geometry with a collector area of 200 cm². (b) Position and normalized magnitude (U_{mag} /U_{ref}) of the maximum flow acceleration above the 400 cm² and 200 cm² collectors, compared with the performance of the aerodynamic EML SBS-500 gauge.

The two scaled versions exhibit very similar behaviour, although the smaller gauge produces a slightly higher and more intense separation layer. This suggests that rigorous scaling cannot be achieved, with performance increasing slightly as the collector's area increases. Nevertheless, the differences are minimal, and both versions significantly outperform the commercial aerodynamic gauge.

To better highlight the wind-induced bias of the two versions, Fig. 9 shows a comparison of their CRs obtained for liquid particles and plotted against the undisturbed wind speed. The two gauges exhibit almost identical CR curves throughout the investigated range of wind speeds, with the larger gauge showing slightly higher CRs for the smallest drop diameter (0.25 mm), in line with the slightly lower acceleration reported above. Meanwhile, the smaller gauge shows slightly higher CR values for drop diameters of at least 0.5 mm and for strong winds of at least 10 m/s. This suggests that the larger flow

https://doi.org/10.5194/egusphere-2026-2108
Preprint. Discussion started: 12 August 2026

disturbance produced by the smaller gauge is partially offset by its smaller collector area. This is because raindrops need to travel a shorter distance before entering the collector, meaning they have less time to be diverted by the aerodynamic effect.

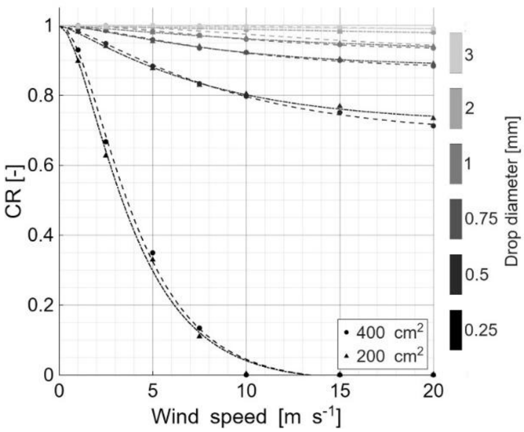

Figure 9: Comparison between the CR values of the design and scaled geometries as a function of wind speed for drop diameters between 0.25 and 3 mm. The dashed and dot-dashed lines show the best-fit functions defined in Eq. (1).

Figure 10a shows a comparison between the CRs of the larger proposed geometry (400 cm^2), and the values of the EML SBS-500 aerodynamic gauge considering liquid precipitation. The proposed geometry consistently outperforms the commercial gauge, with the difference increasing as the wind speed increases. Meanwhile Fig. 10b shows the comparison between the proposed geometry and the AES Nipher shielded gauge considering solid precipitation. In this second case the proposed geometry outperforms the shielded gauge for larger particles while the shielded gauge is better at collecting the smaller ones.

https://doi.org/10.5194/egusphere-2026-2108
Preprint. Discussion started: 12 August 2026

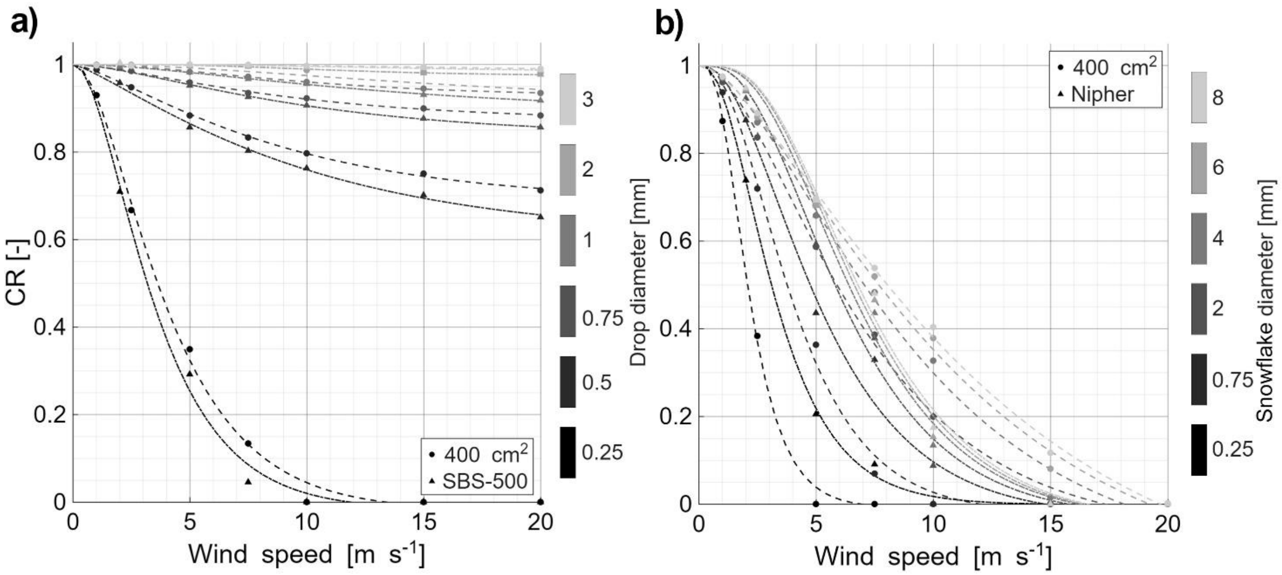

Figure 10: CR values plotted as a function of wind speed for particle diameters between 0.25 and 3 mm. Comparison between the proposed geometry (collector area of 400 cm²) and the aerodynamic EML SBS-500 gauge considering liquid precipitation (a) and the AES Nipher shielded gauge considering solid precipitation (b). The dashed and dot-dashed lines show the best-fit functions defined in Eq. (1).

The residual wind-induced bias in field measurements can be corrected in real time or by applying a posteriori adjustments using the CR values provided in Annex A, once co-located wind measurements are available. To support such procedures, best-fit curves are obtained from the numerical results using a least squares approach. Equation 1 shows the best-fit formulation obtained for the CR as a function of the undisturbed wind speed (U_{ref}), where the three parameters (λ_1, λ_2 and λ_3) depend on the drop diameter (d).

$$CR(d, U_{ref}) = 1 - \lambda_1(d) \cdot \left(1 - exp(-\lambda_2(d)) \cdot U_{ref}\right)^{\lambda_3(d)}, \quad (1)$$

The three parameters, generically indicated as $\lambda_i(d)$, are presented in Table 1 along with their respective Pearson's coefficients.

Table 1: Numerical best-fit parameters of Eq. (1) and their respective Pearson's coefficients (R^2) for gauges with the proposed design and collector areas of 400 cm² and 200 cm².

	Collector area: 400 cm^2										
d[mm]	0.25	0.5	0.75	1	2	3	4	5	6	7	8

λ_1	1.020	0.313	0.128	0.073	0.019	0.017	48.654	0.004	0.002	0.001	0.002
λ_2	0.352	0.134	0.139	0.157	0.574	0.107	0.000	0.114	0.301	0.283	0.619
λ_3	2.176	1.417	1.672	2.560	133.193	4.445	1.935	5.614	30.131	8.630	20.401
R^2	0.996	0.998	0.998	0.999	0.974	0.998	0.912	0.999	0.995	0.957	0.939
Collector area: 200 cm^2											
d[mm]	0.25	0.5	0.75	1	2	3	4	5	6	7	8
λ_1	1.020	0.280	0.119	0.078	2.166	0.114	0.046	0.104	0.048	0.009	0.110
λ_2	0.344	0.143	0.143	0.086	0.000	0.000	0.001	0.000	0.001	0.049	0.000
λ_3	1.884	1.252	1.537	1.280	0.769	0.399	0.503	0.532	0.490	0.518	0.505
R^2	0.996	0.997	0.996	0.996	0.895	0.929	0.985	0.974	0.982	0.989	0.965

Although the catch ratios are the primary result of numerical simulations, they cannot be directly used to adjust raw measurements of integral precipitation variables, including the precipitation intensity (PI), in windy conditions. Indeed, traditional catching type gauges only measure the total volume of precipitation within a given period, whereas the wind-induced bias strongly depends on the size distribution of individual hydrometeors. This makes the bias dependent on the local conditions at the measurement site, especially the precipitation climatology (type and characteristics of events at different precipitation rates).

To adjust PI measurements, the integral effect of wind-induced bias of individual hydrometeors is calculated, typically expressed in the form of the Collection Efficiency (CE). It represents the ratio between the volume of precipitation collected by the gauge in windy conditions and the volume of precipitation that would have been collected if no aerodynamic disturbance was present. The CE can be calculated using Eq. (2):

$$CE\left(d,U_{ref}\right)=\frac{\int_0^{d_{max}}\rho_p\,V_p(d)\;CR\left(d,U_{ref}\right)N(d,RI)\,\mathrm{d}d}{\int_0^{d_{max}}\rho_p\,V_p\;N(d,RI)\,\mathrm{d}d}, \quad (2)$$

where ρ_p is the particle density, $V_p(d)$ is the volume of the particle of equivolumetric diameter d and $N(d,RI)$ represents the particle size distribution (PSD), i.e. the numerosity of particles of equivolumetric diameter d in a cubic meter of air during a precipitation event of intensity PI.

This work does not refer to any specific measurement site. To make the performance assessment as general as possible, we consider a hypothetical site where the relationship between the number of hydrometeors of a given size and precipitation intensity is known and can be assumed to follow the formulation proposed by Marshall and Palmer (1948). This simple yet

https://doi.org/10.5194/egusphere-2026-2108
Preprint. Discussion started: 12 August 2026

physically based PSD formulation is used here as an example but could be replaced by a PSD tailored to a specific measurement site and climatology. The general form of the Marshall–Palmer distribution is a negative exponential, where the scale parameter N_0 and the shape parameter Λ are functions of precipitation intensity. The following expressions are provided for the dependence of parameters on rainfall intensity (RI), following Marshall & Palmer (1948):

$$N_0 = 8000 \text{ (mm}^{-1}\text{ m}^{-3}\text{)}, \tag{3}$$

$$\Lambda = 4.1 \cdot RI^{-0.21} \text{ (mm}^{-1}\text{)}, \tag{4}$$

For snow, we adopted the formulations of the two parameters as a function of snowfall intensity (SI) as proposed by Gunn and Marshall (1958):

$$N_0 = 3.8 \cdot 10^3 \cdot SI^{-0.87} \text{ (mm}^{-1}\text{ m}^{-3}\text{)} \tag{5}$$

$$\Lambda = 25.5 \cdot SI^{-0.48} \text{ (cm}^{-1}\text{)} \tag{6}$$

The CE was computed for the simulated wind speeds and eight values of RI between 1 mm h^{-1} and 500 mm h^{-1}, while for snow SI was from 0.1 to 50 mm h^{-1}. The obtained numerical values of the CE were fitted using Eq. (7) against the associated Precipitation Intensity (PI), with three parameters A, B and C. Their values are shown in Table 2 alongside their respective Pearson's coefficients.

$$CE(PI, U_{ref}) = 1 - \frac{A(PI)}{1 + \left(C(PI) \cdot U_{ref}\right)^{B(PI)}}, \tag{7}$$

Table 2: Values of the best-fit parameters A, B and C and their corresponding Pearson's coefficient for the proposed gauge shape and rim profile with a collector area of 400 cm^2, for both RI and SI measurements.

	Rainfall Intensity (RI) [mm h^{-1}]							
	1	5	10	20	50	100	200	500
$A(RI)$	0.190	0.156	0.118	0.095	0.075	0.055	0.044	0.036
$B(RI)$	-1.685	-1.660	-1.638	-1.626	-1.618	-1.607	-1.598	-1.587
$C(RI)$	0.159	0.145	0.127	0.115	0.103	0.088	0.078	0.068
R^2	0.9996	0.9996	0.9995	0.9992	0.9985	0.9968	0.9948	0.9924

https://doi.org/10.5194/egusphere-2026-2108
Preprint. Discussion started: 12 August 2026

	Snowfall Intensity (SI) [mm h^{-1}]							
	0.1	0.5	1	2	5	10	20	50
$A(SI)$	1.029	1.061	1.089	1.141	1.222	1.275	1.316	1.352
$B(SI)$	-2.437	-2.194	-2.042	-1.900	-1.787	-1.735	-1.700	-1.671
$C(SI)$	0.341	0.235	0.196	0.160	0.128	0.114	0.105	0.098
R^2	0.9974	0.9957	0.9971	0.9969	0.9956	0.9953	0.9954	0.9958

The parameters A, B and C are a function of PI and were fitted using Eq. (8), Eq. (9) and Eq. (10), respectively. The values of the best-fit parameters and their Pearson's coefficients are provided in Table 3.

$$A(PI) = m_A(1 + PI)^{-n_A}, \tag{8}$$

$$B(PI) = m_B - \frac{1}{PI^{n_B}}, \tag{9}$$

$$C(PI) = m_U \cdot PI^{n_U}, \tag{10}$$

Table 3: Numerical best-fit parameters of Eq. (8), (9) and (10) and their respective Pearson's coefficients (R^2) for a gauge with the proposed design and a collector area of 400 cm^2, considering both liquid and solid precipitation.

Collector area: 400 cm^2	$A(PI)$			$B(PI)$			$C(PI)$		
	m_A	n_A	R^2	m_B	n_B	R^2	m_U	n_U	R^2
Liquid precipitation	0.260	0.407	0.9878	0.658	0.013	0.8326	0.158	-0.152	0.9940
Solid precipitation	1.060	-0.045	0.9003	1.214	0.172	0.9136	0.253	-0.218	0.8906

The resulting CE curves are shown in Fig. 11 for the proposed optimal design of the gauge with collector area of 400 cm^2. The performance obtained is compared with that of the aerodynamic EML SBS-500 gauge for rain measurements and with that of the AES Nipher shielded gauge for snow measurements. As expected, the CE decreases with increasing the undisturbed wind speed since the aerodynamic disturbance increases, as already shown for the CR curves. Meanwhile, the CE increases with increasing RI, due to the higher number of large-size particles (less influenced by wind) that are present in intense precipitation.

https://doi.org/10.5194/egusphere-2026-2108
Preprint. Discussion started: 12 August 2026

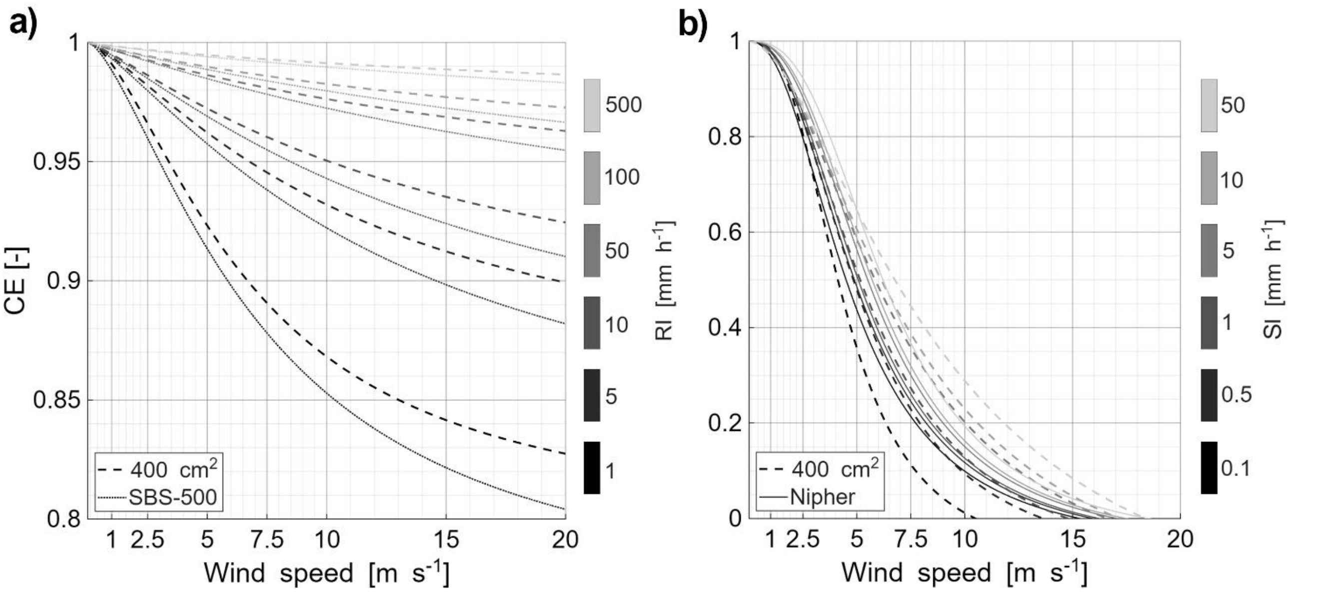

Figure 11: CE curves as a function of the undisturbed wind speed for different PI values (greyscale bar) considering a collector area of 400 cm^2. The CE is compared with that of the aerodynamic EML SBS-500 gauge for rain (a) and the AES Nipher shielded gauge for snow (b).

In case of rainfall measurements, the CE of the proposed gauge design outperforms the existing aerodynamic gauge at any wind speed and rainfall intensity. Meanwhile in the case of snowfall measurements, the proposed geometry shows larger variability depending on the SI than the AES Nipher shielded gauge. For low SI the shielded gauge outperforms the proposed geometry up to about 1 mm h^{-1}, for stronger SI instead, the proposed geometry performs visibly better than the shielded gauge. This is since the proposed geometry presents larger CR values for larger drops.

5 Conclusions

Existing hardware solutions that aim to minimise wind-induced bias in traditional catching-type rain gauges have focused on either shaping the outer shell into an inverted cone to facilitate airflow separation at collector height or introducing windshields to break the airflow upstream of the gauge. Building on the inverted conical shape and meeting the WMO recommendations to avoid splashing from the collector, we have demonstrated that a suitable aerodynamic rim profile can further enhance the gauge's performance in windy conditions.

CFD simulations of the aerodynamic behaviour of the rim profile allowed us to search for the best performing solution, and to identify it in the dual inclination rim profile with an inflow angle of 45°, an outflow angle of 10° and a normalised arc span (the ratio of the collector diameter to the arc length) of 3. By using this last parameter, the best performing aerodynamic solution can be scaled to gauges having different sizes of the collector's area, with demonstrated similar performance. We

https://doi.org/10.5194/egusphere-2026-2108
Preprint. Discussion started: 12 August 2026

proved in this work that such an aerodynamic design effectively outperforms existing rain gauge design that are commercially available at the time of writing.

To achieve higher measurement accuracy, the residual bias can be eliminated by applying the numerically derived adjustment curves provided in this work to the raw measured data in post-processing. This would require taking measurements at a fine temporal sampling rate, ideally at one-minute intervals, and having co-located anemometer measurements available at the rain gauge station. Since both wind and precipitation are erratic in nature, applying adjustments at a fine temporal scale ensures greater accuracy.

The effect of the aerodynamic design of the outer shell and rim profile is independent of the gauge's measuring principle, since these features only influence the instrument's ability to accurately collect precipitation. The associated bias (wind-induced undercatch) adds to the gauge's counting performance, i.e. its ability to accurately quantify the amount of collected precipitation. Therefore, any mechanical device can be installed inside the shell and below the collector for the instrument to operate as e.g., a tipping-bucket, floating or weighing gauge, as required. To enhance the overall measurement accuracy, it is recommended that any instrumental bias deriving from the adopted measuring principle is also considered, for instance by properly accounting for the systematic mechanical bias of the tipping-bucket mechanism and applying the associated adjustment curves obtained from standardised laboratory testing (Cauteruccio et al., 2021).

The results of this work will support manufacturers of hydrometeorological instruments in achieving higher measurement accuracy. The aerodynamic design of the outer shell and rim profile of rain gauges is important in regions where wind is frequent during precipitation events, and better measurements are needed to provide researchers with reliable datasets that can be used to assess possible trends in precipitation regimes at local and global scales. It should be noted that introducing more accurate instruments to sites with a previous measurement history inevitably introduces inhomogeneities in the historical time series. Countermeasures should therefore be taken to ensure that such changes are interpreted as spurious rather than real climatological signals.

Appendix A

Table 1A: Catch Ratios (CR) obtained from numerical simulations for the 400 cm^2 gauge considering liquid precipitation as a function of drop diameter and wind speed.

				U_{ref}			
D	1 m s^{-1}	2.5 m s^{-1}	5 m s^{-1}	7.5 m s^{-1}	10 m s^{-1}	15 m s^{-1}	20 m s^{-1}
0.25 mm	0.930	0.667	0.350	0.134	0.000	0.000	0.000
0.5 mm	0.988	0.948	0.883	0.834	0.797	0.750	0.713
0.75 mm	0.996	0.985	0.959	0.935	0.922	0.900	0.884
1 mm	1.000	0.997	0.984	0.972	0.960	0.944	0.935

https://doi.org/10.5194/egusphere-2026-2108
Preprint. Discussion started: 12 August 2026

2 mm	0.998	0.999	0.998	0.997	0.988	0.983	0.980
3 mm	1.000	1.000	1.000	0.999	0.997	0.994	0.990
4 mm	1.000	1.000	1.000	0.999	0.999	0.999	0.996
5 mm	1.000	1.000	1.000	1.000	1.000	0.999	0.998
6 mm	1.000	1.000	1.000	1.000	1.000	0.998	0.998
7 mm	1.000	1.000	1.000	1.000	1.000	0.999	0.999
8 mm	1.000	1.000	0.999	0.998	0.998	0.998	0.998

Table 2A: Catch Ratios (CR) obtained from numerical simulations for the 200 cm^2 gauge considering liquid precipitation as a function of drop diameter and wind speed.

				U_{ref}			
CR	1 m s^{-1}	2.5 m s^{-1}	5 m s^{-1}	7.5 m s^{-1}	10 m s^{-1}	15 m s^{-1}	20 m s^{-1}
0.25 mm	0.898	0.627	0.330	0.111	0.003	0.000	0.000
0.5 mm	0.981	0.940	0.877	0.829	0.805	0.769	0.734
0.75 mm	0.995	0.984	0.954	0.940	0.921	0.904	0.890
1 mm	0.997	0.991	0.979	0.969	0.964	0.947	0.940
2 mm	0.995	0.994	0.994	0.993	0.989	0.981	0.980
3 mm	0.996	0.995	0.995	0.994	0.993	0.990	0.990
4 mm	0.998	0.997	0.996	0.995	0.995	0.994	0.992
5 mm	0.998	0.997	0.997	0.995	0.995	0.994	0.992
6 mm	0.998	0.997	0.997	0.996	0.995	0.994	0.993
7 mm	0.998	0.997	0.996	0.995	0.995	0.994	0.993
8 mm	0.998	0.997	0.997	0.996	0.996	0.994	0.993

Table 3A: Catch Ratios (CR) obtained from numerical simulations for the 400 cm^2 gauge considering solid precipitation as a function of snowflake diameter and wind speed.

				U_{ref}			
CR	1 m s^{-1}	2.5 m s^{-1}	5 m s^{-1}	7.5 m s^{-1}	10 m s^{-1}	15 m s^{-1}	20 m s^{-1}
0.25 mm	0.873	0.383	0.000	0.000	0.000	0.000	0.000

https://doi.org/10.5194/egusphere-2026-2108
Preprint. Discussion started: 12 August 2026

0.5 mm	0.915	0.629	0.201	0.000	0.000	0.000	0.000
0.75 mm	0.939	0.720	0.363	0.070	0.000	0.000	0.000
1 mm	0.948	0.767	0.451	0.196	0.003	0.000	0.000
2 mm	0.962	0.836	0.587	0.387	0.200	0.001	0.000
3 mm	0.968	0.852	0.634	0.452	0.286	0.008	0.000
4 mm	0.972	0.870	0.659	0.483	0.327	0.016	0.000
5 mm	0.972	0.875	0.672	0.504	0.357	0.051	0.001
6 mm	0.974	0.882	0.684	0.519	0.379	0.081	0.001
7 mm	0.975	0.884	0.690	0.531	0.392	0.098	0.002
8 mm	0.975	0.891	0.696	0.538	0.403	0.117	0.003

Code and data availability

The numerical simulations upon which this study is based are too large to archive or to transfer. All the information needed to replicate the simulations is however reported within the text or in the Appendix A. The OpenFOAM software used to run simulations is open source and detailed in Jasak (2009).

Author contributions

Conceptualization, A.C., E.C., and L.G.L.; methodology, A.C., E.C., and L.G.L.; software, E.C.; formal analysis, E.C.; investigation, A.C., E.C.; resources, P.W.C. and L.G.L.; data curation, E.C.; writing—original draft preparation, E.C. and A.C.; writing—review and editing, P.W.C. and L.G.L.; visualization E.C., A.C.; supervision, A.C., and L.G.L.; funding acquisition, P.W.C and L.G.L. All authors have read and agreed to the published version of the manuscript.

Competing interests

The authors declare that they have no conflict of interest.

Disclaimer

Copernicus Publications adds a standard disclaimer: “Copernicus Publications remains neutral with regard to jurisdictional claims made in the text, published maps, institutional affiliations, or any other geographical representation in this paper.

While Copernicus Publications makes every effort to include appropriate place names, the final responsibility lies with the authors. Views expressed in the text are those of the authors and do not necessarily reflect the views of the publisher."
Please feel free to add disclaimer text at your choice, if applicable.

Acknowledgements

This work was partially funded by Senseca Italy Ltd., whose support is gratefully acknowledged.

Financial support

This work was partially funded by Senseca Italy Ltd.

Review statement

The review statement will be added by Copernicus Publications listing the handling editor as well as all contributing referees according to their status anonymous or identified.

References

Cauteruccio A., Colli M., Stagnaro M., Lanza L.G. and Vuerich E.: In situ precipitation measurements. In: Foken T. (ed.), Handbook of Atmospheric Measurements. Springer Nature, Switzerland, 359-400. ISBN 978-3-030-52170-7, https://doi.org/10.1007/978-3-030-52171-4_12, 2021.

Cauteruccio, A., Chinchella, E. and Lanza, L.G.: The overall collection efficiency of catching-type precipitation gauges in windy conditions. Water Resources Research, 60(1), e2023WR035098, https://doi.org/10.1029/2023WR035098, 2024.

Colli, M., Pollock, M., Stagnaro, M., Lanza, L.G., Dutton, M. and O'Connell, E.: A Computational Fluid-Dynamics assessment of the improved performance of aerodynamic rain gauges. Water Resour. Res., 54 (2), 779-796, https://doi.org/10.1002/2017WR020549, 2018.

Davis Instruments: *Rain Collector, User Manual*. Davis Instruments, Hayward, CA, USA, 8 pp, http://www.davisinstruments.com, last access: 11 April 2026, 2022.

Dhert, T., Ashuri, T. and Martins, J.R.R.A.: Aerodynamic shape optimization of wind turbine blades using a Reynolds-averaged Navier–Stokes model and an adjoint method. Wind Energy, 20, 909-926, http://doi.org/10.1002/we.2070, 2017.

EML: *SBS Range Rain Gauge, User Manual*. Environmental Measurements Limited (EML) North Shields, United Kingdom, 16 pp, http://www.emltd.net/sbs.html, last access 11 April 2026, 2017.

Folland, C.K.: Numerical models of the raingauge exposure problem, field experiments and an improved collector design. Quarterly Journal of the Royal Meteorological Society, 114(484), 1485-1516, https://doi.org/10.1002/qj.49711448407, 1988.

https://doi.org/10.5194/egusphere-2026-2108
Preprint. Discussion started: 12 August 2026

Green, M.J. and Helliwell, P.R.: The effect of wind on the rainfall catch. In: *Distribution of precipitation in mountainous areas. Geilo Symposium, Norway (31 July – 5 August 1972)*, WMO Report No. 326; World Meteorological Organization, Geneva, Switzerland, Vol. 2, pp. 27–46, https://library.wmo.int/idurl/4/37673, last access:11 April 2026, 1972.

Gunn, K.L.S., and Marshall, J.S.: The distribution with size of aggregate snowflakes. J. Meteor., 15, 452–461, https://doi.org/10.1175/1520-0469(1958)015,0452:TDWSOA.2.0.CO;2, 1958.

Habib, E., Krajewski, W.F., Nespor, V. and Kruger, A.: Numerical simulation studies of rain gage data correction due to wind effect. *Journal of Geophysical Research: Atmospheres*, *104*(D16), 19723-19733, https://doi.org/10.1029/1999JD900228, 1999.

Hasse, L., Grossklaus, M., Uhlig, K. and Timm, P.: A ship rain gauge for use in high wind speeds. Journal of Atmospheric and Oceanic Technology, 15(2), 380-386, https://doi.org/10.1175/1520-0426(1998)015<0380:ASRGFU>2.0.CO;2, 1998.

He, X., Li, J., Mader, C.A., Yildirim, A. and Martins, J.R.R.A.: Robust aerodynamic shape optimization—From a circle to an airfoil. Aerospace Science and Technology, 87, 48-61, https://doi.org/10.1016/j.ast.2019.01.051, 2019.

Jasak, H.: OpenFOAM: Open source CFD in research and industry. *International Journal of Naval Architecture and Ocean Engineering*, 1(2), 89–94, https://doi.org/10.2478/IJNAOE-2013-0011, 2009.

Jeanmasson, G., Mary, I. and Mieussens, L.: On some explicit local time stepping finite volume schemes for CFD. Journal of Computational Physics, 397, 108818, https://doi.org/10.1016/j.jcp.2019.07.017, 2019.

Kochendorfer, J., Rasmussen, R., Wolff, M., Baker, B., Hall, M.E., Meyers, T., Landolt, S., Jachcik, A., Isaksen, K., Brækkan, R., et al.: The quantification and correction of wind-induced precipitation measurement errors. Hydrol. Earth Syst. Sci., 21, 1973–1989, https://doi.org/10.5194/hess-21-1973-2017, 2017.

Lindroth, A.: Reduced loss in precipitation measurements using a new wind shield for raingages. *Journal of Atmospheric and Oceanic Technology*, *8*(3), 444-451, https://doi.org/10.1175/1520-0426(1991)008<0444:RLIPMU>2.0.CO;2, 1991.

Liu, F.: A thorough description of how wall functions are implemented in OpenFOAM. In: *Proceedings of CFD with OpenSource software*, *34*, 1-33. Edited by Nilsson. H., Available at: https://www.tfd.chalmers.se/~hani/kurser/OS_CFD_2016/FangqingLiu/openfoamFinal.pdf, last access: 11 April 2026, 2016.

Marshall, J.S. and Palmer, W.M.K.: The distribution of raindrops with size. Journal of Atmospheric Sciences, 5(4), 165-166, https://doi.org/10.1175/1520-0469(1948)005<0165:TDORWS>2.0.CO;2, 1948.

Martins, J.R.R.A.: Aerodynamic design optimization: Challenges and perspectives. Computers & Fluids, 239, 105391, https://doi.org/10.1016/j.compfluid.2022.105391, 2022.

Menter, F.R.: Two-equation eddy-viscosity turbulence models for engineering applications. AIAA journal, 32(8), 1598-1605, https://doi.org/10.2514/3.12149, 1994.

Nešpor, V. and Sevruk, B.: Estimation of wind-induced error of rainfall gauge measurements using a numerical simulation. Journal of atmospheric and oceanic technology, 16(4), 450-464, https://doi.org/10.1175/1520-0426(1999)016<0450:EOWIEO>2.0.CO;2. 1999.

https://doi.org/10.5194/egusphere-2026-2108
Preprint. Discussion started: 12 August 2026

Nipher, F.E.: On the determination of the true rainfall, by elevated gages. Proceedings of the American Association for the Advancement of Science, St. Louis, 1878, p. 103–08. https://doi.org/10.1016/0022-1694(77)90001-4, last access: 11 April 2026, 1878.

Nitu, R. and Wong, K.: CIMO survey on national summaries of methods and instruments for solid precipitation measurement at automatic weather stations. WMO IOM Rep. n. 102, WMO/TD-No. 1544, World Meteorological Organisation (WMO), 57 pp., Geneva, Switzerland, https://library.wmo.int/idurl/4/50474, last access: 11 April 2026, 2010.

Pironneau, O.: On optimum design in fluid mechanics. J. Fluid Mechanics. 1974;64(1):97-110, https://doi.org/10.1017/S0022112074002023, 1974.

Rasmussen, R., Vivekanandan, J., Cole, J., Masters, B.M.C. and Masters, C.: The estimation of snowfall rate using visibility. Journal of Applied Meteorology, 38(10), 1542–1563, https://doi.org/10.1175/1520-0450(1999)038%3C1542:TEOSRU%3E2.0.CO;2, 1999.

Robinson, A.C. and Rodda, J.C.: Rain wind and the aerodynamic characteristics of rain gauges. *Meteorol. Mag.*, 98, 113-120, https://digital.nmla.metoffice.gov.uk/IO_f2d242ba-7c17-4b78-837e-6a6beede3736/, last access: 11 April 2026, 1969.

Seibert, J. and Morén, A.S.: Reducing systematic errors in rainfall measurements using a new type of gauge. Agricultural and Forest Meteorology, 98, 341-348, https://doi.org/10.1016/S0168-1923(99)00107-0, 1999.

Strangeways, I.: Improving precipitation measurement. *International Journal of Climatology: A Journal of the Royal Meteorological Society*, *24*(11), 1443-1460, https://doi.org/10.1002/joc.1075, 2004.

WMO: *Guide to Instruments and Methods of Observation* (WMO-No. 8). Geneva, 2021–2025, https://library.wmo.int/idurl/4/41650, last access: 09 April 2026, 2024.